JOURNAL OF PROPULSION AND POWER
Vol. 9, No. 6, Nov.-Dec. 1993

Full Navier-Stokes Analysis of an Axisymmetric Scramjet Inlet

Yeu-Chuan Hsia*
Rockwell International Corporation, Canoga Park, California 91309

A full Navier-Stokes (FNS) computation was carried out on a mixed-compression axisymmetric scramjet inlet at Mach 5. The geometry including a blunt nose and cowl leading edge was modeled using a multizone approach which permitted running either time-marching or space-marching on individual zones. A Baldwin-Lomax turbulence model was used to simulate the effects of turbulence. The flow solution agreed very well with the test data on the wall static pressure and throat total pressure. The inlet performance calculated by postprocessing the solution matched the wind-tunnel test data as well.

I. Introduction

RAMJET and scramjet (supersonic combustion ramjet) engines are promising propulsion devices for the air-breathing hypersonic vehicles. These engines are mechanically simpler than the turbojet-type engines, yet they operate more efficiently at supersonic and hypersonic speeds. Due to the wide range of speeds and altitudes of hypersonic flight, the development and design of these engines face some inherent difficulties. The ground test facilities can usually operate at a limited number of discrete conditions for a very short duration. Besides, the enormous power required to operate the facility limits the size of the facility and, in turn, the size of the model. As a result, these facilities cannot simulate the full range and scope of the flight regime.

Computational fluid dynamics (CFD), which uses numerical algorithms to solve fluid dynamics equations on computers, has become a powerful tool to complement the ground testing and to extrapolate to the flight conditions. In the past two decades, numerical algorithms have been advanced from solving the potential equations to the full Navier-Stokes (FNS) equations with chemical reactions. Numerical techniques were also developed to simulate flowfields of multiple engine modules[1] and engine/airframe integrated vehicles.[2] However, the capabilities of the computer codes based on these techniques were usually demonstrated with simplified geometries. Code validations on more complex flowfields are needed. The objective of the present work is to validate the CFD code on a more realistic configuration.

This article is to report a full Navier-Stokes analysis on the inlet of the hypersonic research engine (HRE), which was designed and tested in the late 1960s. Two scaled models of the HRE inlet were tested extensively in the wind tunnels.[3] Some of the test data are used here for CFD validation.

II. Model Geometry and Wind-Tunnel Test

The inlet is an axisymmetric, mixed-compression design with a translating cowl to control the compression (Fig. 1). It is composed of two parts: 1) the centerbody and 2) the cowl. The present analysis involves only zero angle of attack and zero yaw, hence the flow can be assumed to be axisymmetric and only a single azimuthal plane needs to be computed. A two-dimensional Cartesian coordinate is used with the X axis being the axial coordinate along the centerline, and the Y axis being the radial coordinate. The origin is located at the imaginary vertex of the conical centerbody. The dimensions shown in Fig. 1 have been nondimensionalized by the cylindrical cowl radius at the leading edge R_c.

The wind-tunnel tests were made at various Mach numbers between 4–8 on two scaled models: 1) one-third scale and 2) two-thirds scale. The current analysis was based on the two-thirds scaled model tested at tunnel Mach number of 5. The cowl leading edge (X_{CL}) was set at $3.865R_c$. The tunnel total pressure and total temperature were 40 psia and 665°R, respectively. The Reynolds number per foot was 1.84×10^6. The model was cooled to 460°R. No boundary-layer trip was used, and the boundary-layer transition on the centerbody was estimated[3] at $X/R_c = 3.3$. During the test, the inlet was started, i.e., the core flow was supersonic throughout the inlet. The available test data for CFD validation were in the forms of wall static pressure distributions, throat total pressure profiles, air capture ratio, and total pressure recovery.

III. Computation Setup

A. CFD Code

The FNS solver used is the USA-RG2 (unified solution algorithm, real gas, two-dimensional), one of the USA series of codes.[2] These codes have been used to solve a variety of fluid dynamics problems.[4,5] The USA-RG2 solves the two-dimensional or axisymmetric conservation law form of the time-dependent full Navier-Stokes or, in the case of turbulence, the Reynolds-averaged Navier-Stokes (RANS) equations based on the finite volume discretization using the TVD formulation[6] to capture strong discontinuities (or shock waves) without spurious oscillations. The solution methodologies used in the code include a multistage Runge-Kutta explicit scheme, the approximate factorization scheme, and the Gauss-Seidel and colored relaxation schemes. The code can be run in either time- or space-marching mode. The gas properties can be

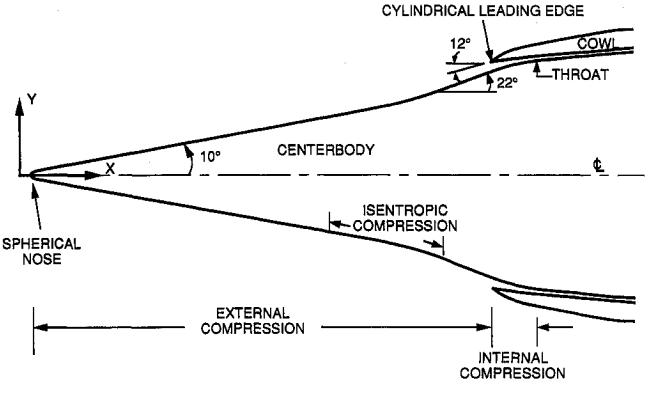

Fig. 1 Schematic of the axisymmetric inlet.

Received March 9, 1992; presented as Paper 92-3100 at the AIAA /SAE/ASME/ASEE 28th Joint Propulsion Conference, Nashville, TN, July 6–8, 1992; revision received May 8, 1993; accepted for publication May 14, 1993.

*Member Technical Staff, Rocketdyne Division. Member AIAA.

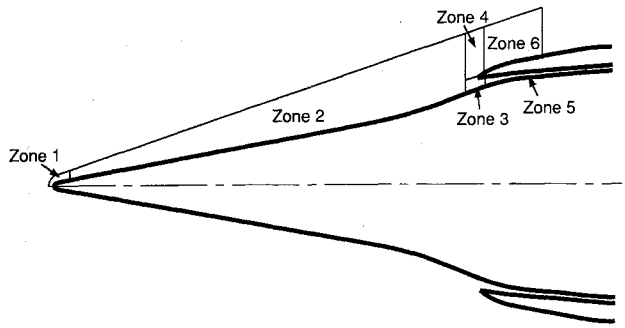

Fig. 2 Computation zonal arrangement.

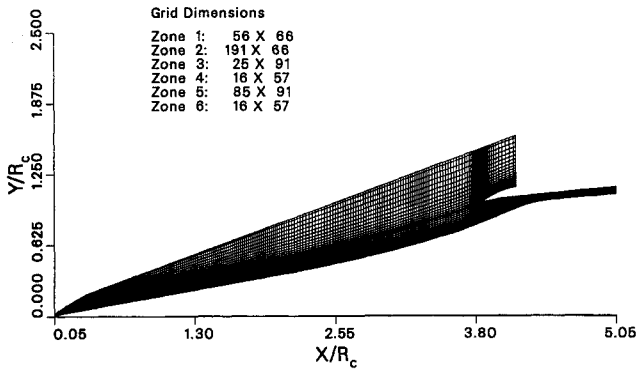

Fig. 3 6-Zone computation grid.

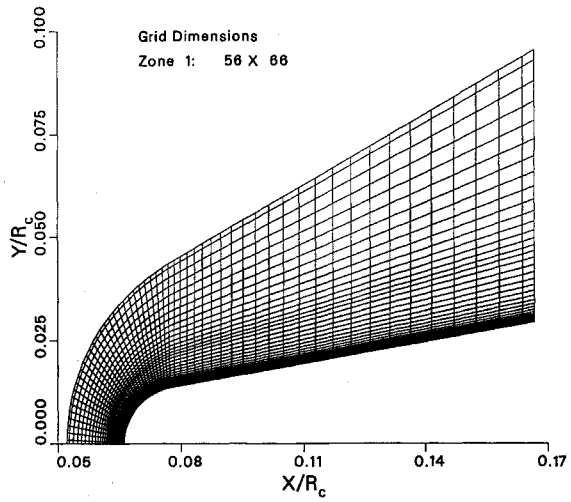

Fig. 4 Zone 1 grid around centerbody nose.

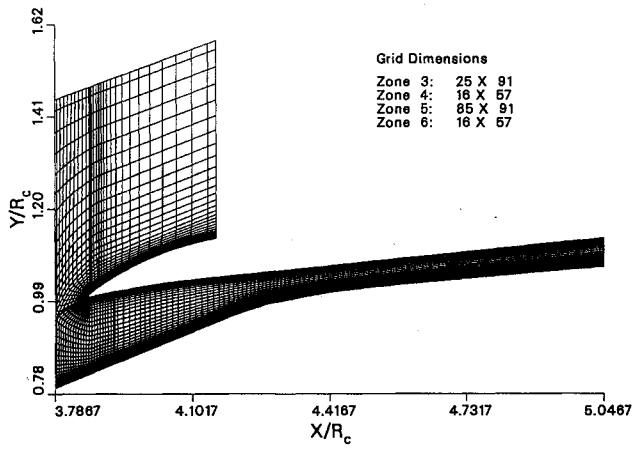

Fig. 5 Grids around cowl and in the internal compression region (zones 3–6).

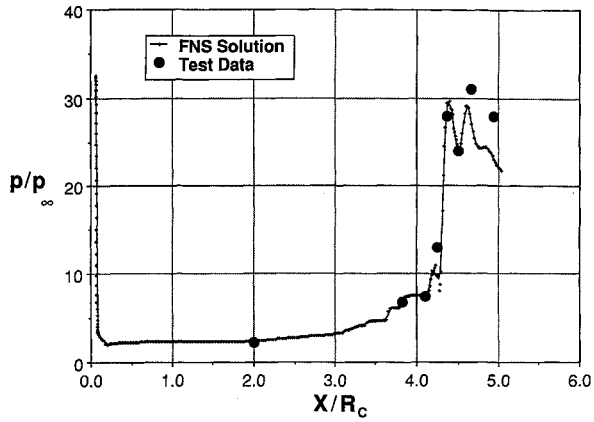

Fig. 6 Centerbody wall static pressure distribution.

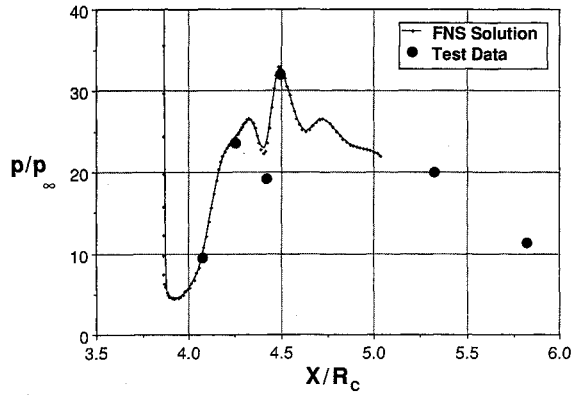

Fig. 7 Cowl internal wall static pressure distribution.

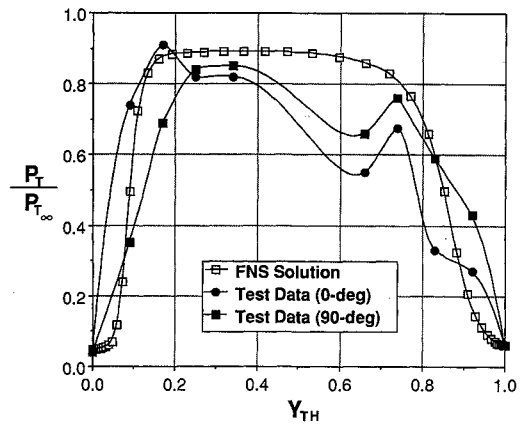

Fig. 8 Throat total pressure profile.

chosen from perfect gas or real gas. The real gas option allows for equilibrium air,[7] frozen chemistry, and finite-rate chemistry.[8] The solver incorporates three turbulence models: 1) a zero-equation Baldwin-Lomax model, 2) a one-equation turbulent kinetic energy transport model,[9] and 3) a two-equation k-ε transport model.[10] The code also possesses a multizone structured grid bookkeeping capability which facilitates the treatment of complex geometries.[11]

In the current analysis, the axisymmetric option of the code was selected and the perfect gas property was assumed. Both time-marching and space-marching methods were used. The time-marching method used was the approximate factorization scheme with scalar tridiagonal left side. The space-marching method used was the Gauss-Seidel relaxation scheme. For the zones with turbulent flows, the Baldwin-Lomax turbulence model was selected. Although the original Baldwin-Lomax model was derived based on the incompressible flow, the one used in the USA code carried the compressibility

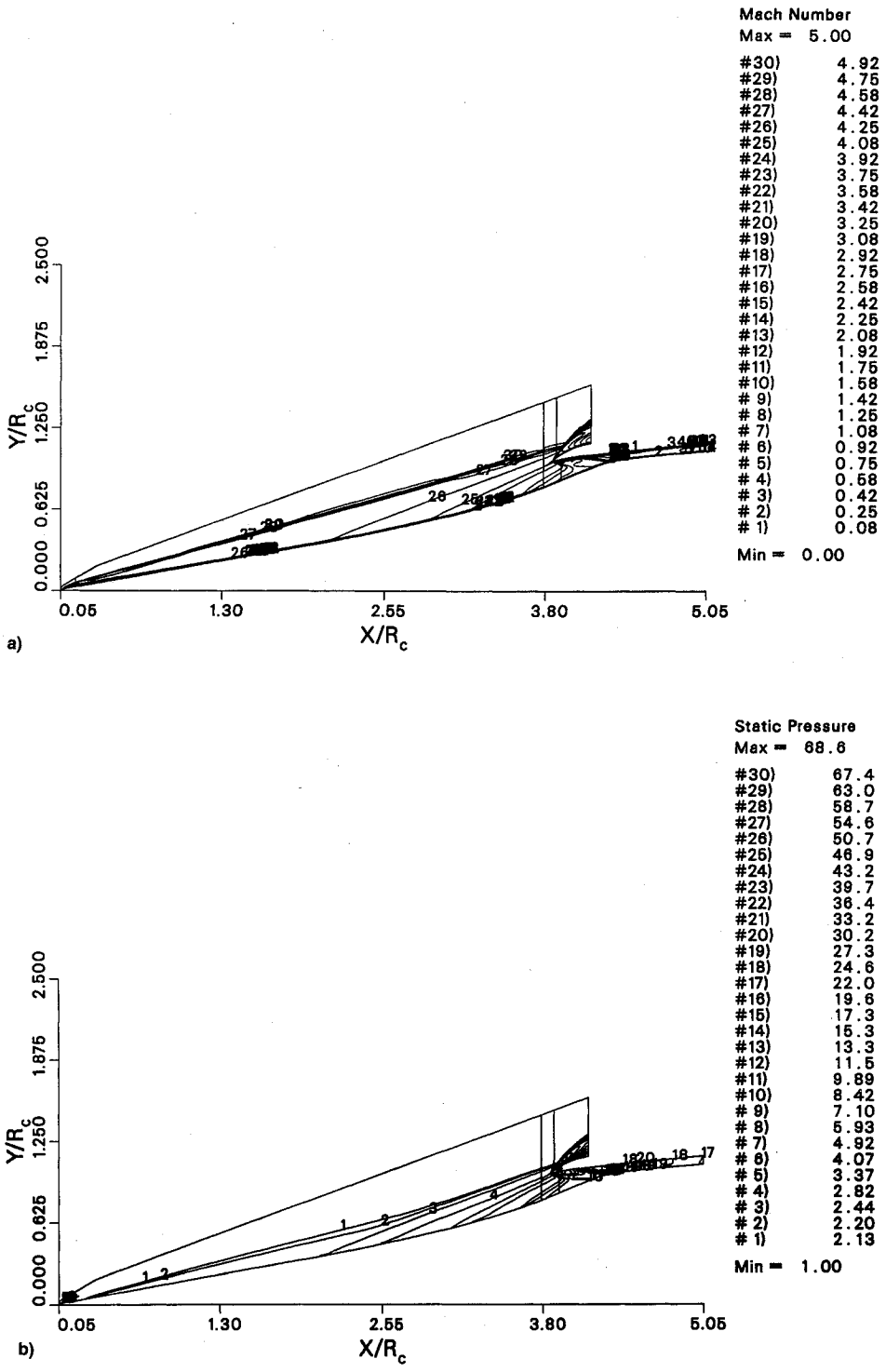

Fig. 9 Overall inlet flowfield: a) Mach number contours and b) normalized static pressure contours.

effect through the use of constants based on the compressible flow.

B. Grid System

Six zones were used in this analysis (Fig. 2) to handle the complex flowfield. Zone 1 modeled the blunt nose of the centerbody. Zone 2 covered most of the external compression region. Zones 3 and 4 defined the geometry of the cowl lip. Zone 5 was the internal compression region. Zone 6 took care of the flow external of the cowl. The total number of grid nodes was 28,136 (Fig. 3). The exact circular geometries of the nose and cowl lip were modeled (Figs. 4 and 5, respectively). Grids were clustered near the solid surfaces to resolve the boundary-layer flow profiles. The first grid node away from the wall in the throat was about $5.8 \times 10^{-7} R_c$, which corresponded to a y^+ of about 0.01.

C. Boundary Conditions

Boundary conditions are required on all boundaries of each zone. A freestream boundary condition was applied at the upper boundaries of zones 1, 2, 4, and 6. A no-slip boundary condition was used on solid surfaces. A symmetry boundary condition was used on the $Y/R_c = 0.0$ boundary in zone 1. A zero-gradient extrapolation boundary condition was used at the flow exit planes of zones 5 and 6. The boundary conditions used at the zonal connections are either "coupled" or "uncoupled," depending on the orientation of the boundary, the flow physics, and the computation procedure. The coupled

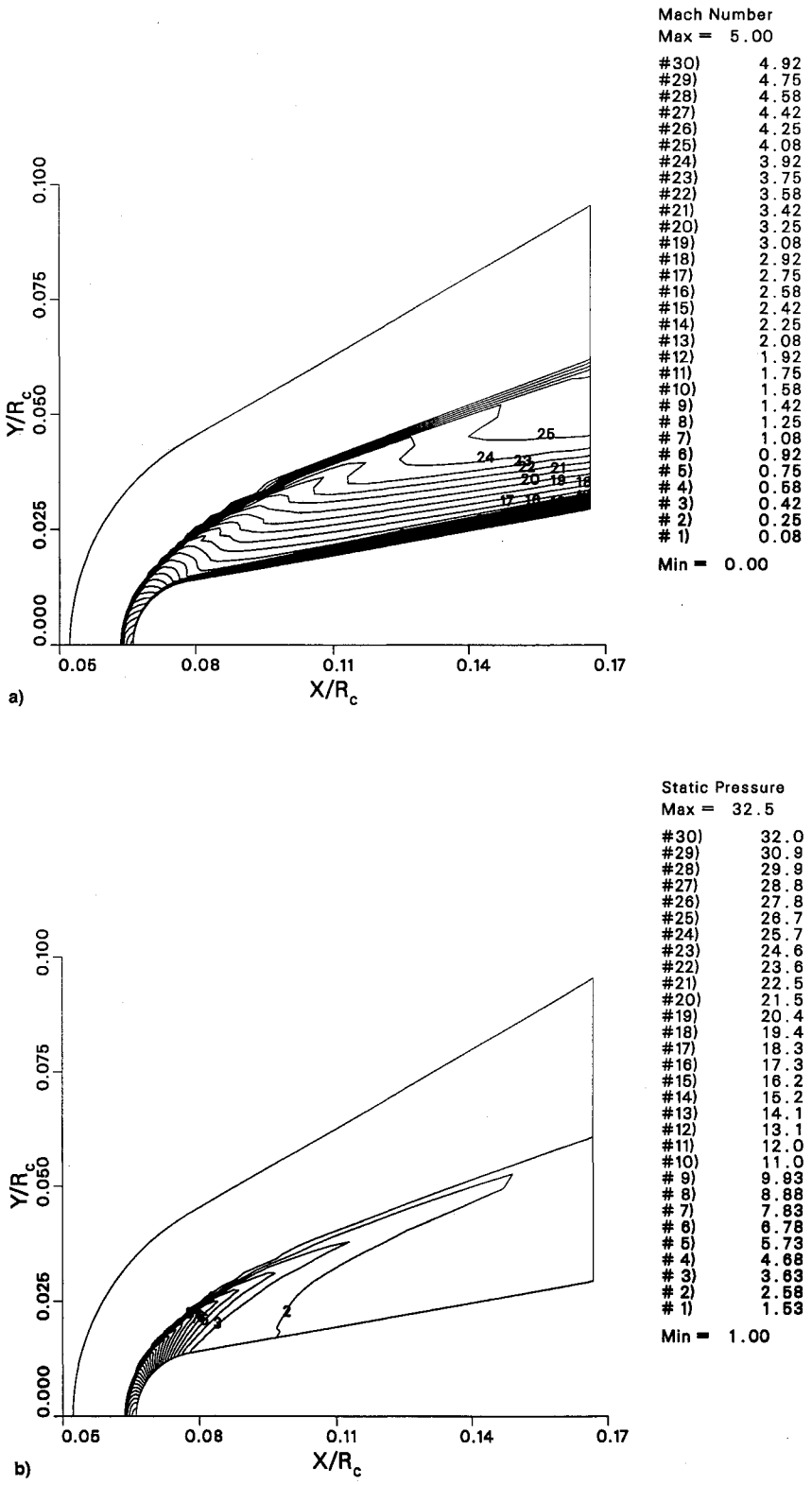

Fig. 10 Centerbody nose flowfield: a) Mach number contours and b) normalized static pressure contours.

zonal boundary condition allows the information to exchange between the neighboring zones. The uncoupled zonal boundary condition allows the flow information to propagate in the forward direction only.

D. Computation Procedure

Because supersonic flows do not propagate downstream influence to upstream, zones connected in the streamwise direction were run sequentially in the flow direction for savings in CPU time. Within each zone, the space-marching method was used unless a subsonic region was expected inside that zone. Zone 1 was first run with time-marching method because subsonic flow was expected at the blunt nose. However, the flow accelerates to supersonic before reaching the downstream boundary. Hence, a zero-gradient extrapolation boundary condition was applied when running zone 1 alone. After zone 1 was converged, its exit flow was used as the

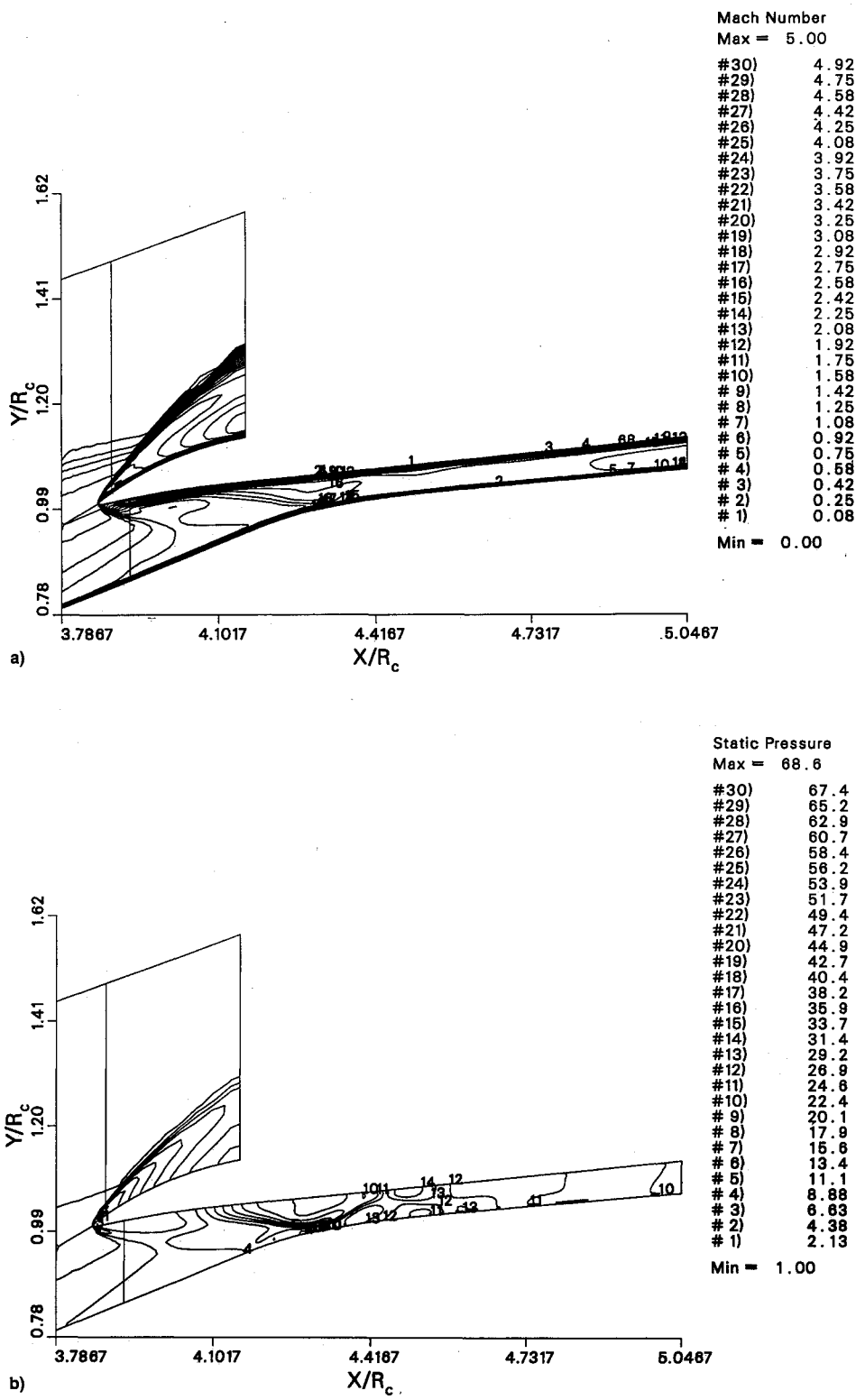

Fig. 11 Flowfield around cowl and internal compression region: a) Mach number contours and b) normalized static pressure contours.

inflow condition for zone 2, which was run with space-marching method. Zones 3 and 4 were then initialized with zone 2 exit flow and run time-marching simultaneously because of the blunt cowl leading edge. Zones 5 and 6, which followed zones 3 and 4, respectively, were run with space-marching method. After every individual zone was computed, all six zones were run time-marching simultaneously with coupled inter-zonal boundary condition to allow interactions between the zones and to have better connectivity.

IV. Numerical Solutions

A. Comparison with Test Data

The comparisons of the CFD solution and test data are shown in Figs. 6–8. Figure 6 shows the normalized wall static pressure along the centerbody. The pressure is high at the tip due to the bluntness of the nose. It drops rapidly past the nose and then increases gradually along the centerbody in the external compression region ($0.066 < X/R_c < 3.865$). In the internal compression region, the pressure first rises sharply

to about 3.5 times the upstream pressure and then reveals an oscillatory behavior. This is typical of a shock train pressure profile in the internal compression inlet. The agreement between the solution and test data is very good except in the region downstream of the throat (i.e., $X/R_c > 4.5$), where the numerical solution shows lower pressures than the test data.

Figure 7 shows the normalized wall static pressure profile on the cowl internal surface. Similar to the nose pressure, the cowl leading edge pressure is very high. It drops rapidly to about 5 and then rises again. It is followed by an oscillatory behavior. Again, the agreement between the solution and test data is good, except the overprediction at $X/R_c = 4.4$. The two data points, which are downstream and outside of the computational domain, seem to be on the trace of the profile of the numerical solution.

Figure 8 shows the total pressure profile across the throat. The vertical axis is the total pressure normalized with the freestream total pressure. The horizontal axis Y_{TH} is the normalized height in the throat [i.e., $(Y - Y_{CB})/H_{TH}$, which is the Y coordinate above the centerbody Y_{CB}, and normalized with the throat height H_{TH}]. Together with the FNS solution, there are two sets of test data shown. Those are test data at 0- and 90-deg azimuthal angles, respectively. They show the imperfect axisymmetry in the testing—the throat core flow skewed towards the centerbody at 0 deg and towards the cowl at 90 deg. Near the centerbody ($0.0 < Y_{TH} < 0.2$), the numerical solution falls in between the two sets of data. On the cowl side ($0.6 < Y_{TH} < 1.0$), the solution failed to predict the low total pressure at $Y_{TH} = 0.65$ and the double inflection around $Y_{TH} = 0.87$. The highly distorted profiles of the test data might be caused by the interactions of boundary layer and shock waves. The failure of capturing the shock waves might be due to the coarse grid in the core flow region.

B. Flowfield Study and Discussion

Figures 9a and 9b show the overall inlet flowfield in terms of Mach number and static pressure ratio (p/p_∞) contours, respectively. The pressure contours in Fig. 9b are weighted towards lower values so that the pressure field of the external compression region can be seen. In Fig. 9a, the clustered Mach contours which extend from nose to the cowl external region indicate the bow shock. The bow shock angle is about 15.5 deg, which is very close to that of the flow past a 10-deg sharp cone.[12] This is expected because the blunt nose is small compared with the centerbody. The flow behind the bow shock continues to be compressed through the isentropic compression section until it reaches the cowl. The flow is still supersonic in front of the cowl (Mach 3.9), thus a cowl shock is generated. Outside of the cowl, it coalesces with the centerbody bow shock. Inside, a shock train is formed. No boundary-layer trip was used on the model centerbody during the wind-tunnel test. It means that the boundary layer transition from laminar to turbulent, if occurred, happened naturally. In the test, the boundary-layer transition was estimated at $X/R_c = 3.3$. The USA code is able to simulate a boundary-layer transition from laminar to turbulent. However, the transition location or region needs to be specified because there is no transition model or criterion incorporated in the code. In the present computation, the transition was set from $X/R_c = 3.1$ to 3.3.

Although the blunt nose has insignificant effects on the overall flowfield, the local heating and stress become significant at hypersonic speeds. Figures 10a and 10b show the Mach number and static pressure contours around the nose. The bow shock is seen very clearly. On the centerline (i.e., $Y/R_c = 0.0$), the bow shock is normal to the flow. The flow behind the shock is subsonic with a Mach number of about 0.4. The pressure jump across the shock is about 29. The temperature behind the normal shock is about six times the freestream temperature. These are very close to the normal shock relations at Mach 5.[12]

Figures 11a and 11b show the flow around the cowl and the internal compression region (zones 3–6). The bow shock is outside the cowl. The flow reaching the cowl leading edge has been compressed by the external compression. At the blunt cowl leading edge, the flow is compressed again to a pressure ratio of 68.6. The part of air that flows into the internal compression region is the captured air, which continues to be compressed through a shock train until it reaches the throat (at $X/R_c = 4.5$). In the computation, the boundary layer was assumed to be laminar on the cowl and turbulent on the centerbody. The maximum Mach number in the throat is 2.6 and the mean Mach number is about 2.3. The mean normalized pressure in the throat is 25.6.

V. Performance Calculations

Inlet performance is often characterized by the air capture ratio (ACR), total pressure recovery (PR) and kinetic energy efficiency (η_{ke}). For a quasi-one-dimensional inlet (Fig. 12), these performance parameters can be defined as

$$\text{ACR} = \frac{\dot{m}_2}{\dot{m}_1} = \frac{\rho_2 V_2 A_2}{\rho_1 V_1 A_1}$$

$$\text{PR} = \frac{P_{T_2}}{P_{T_1}}$$

$$\eta_{ke} = \frac{V_3^2}{V_1^2}$$

where $\dot{m}$ is the mass flow rate, ρ the density, V the velocity, A the cross-sectional area, and P_T the total pressure. The subscripts denote the stations. Station 1 is the uniform inflow plane and station 2 is the throat. V_3 is the velocity that the flow in the throat would obtain if it were isentropically expanded to the inflow (station 1) pressure.

For the present axisymmetric inlet flow, integral and averaged properties are used to make an equivalent one-dimensional flow so that the performance can be calculated using the above definitions. This is done by equating a one-dimensional flow that possesses or conserves the mass, momentum, and energy of the axisymmetric flow in the throat. An averaged throat Mach number ($\bar{M}_2$) can be found by solving a quadratic equation. Other mean quantities, such as $\bar{p}_2$, $\bar{\rho}_2$, and $\bar{V}_2$ are then derived from this Mach number.[13,14]

The computed values of ACR, $\bar{M}_2$, PR and η_{ke} are tabulated together with test data in Table 1. The performance data

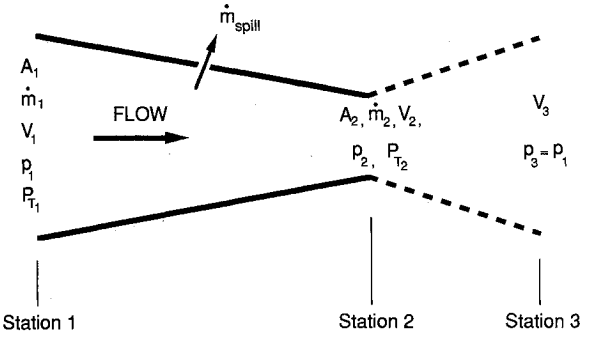

Fig. 12 Nomenclatures for inlet performance calculation.

Table 1 Computed inlet performance compared with test data

	CFD	Test
$\bar{M}_2$	2.33	NA
PR	0.633	0.665
η_{ke}	0.972	NA
ACR	0.853	0.856

available from the test are PR and ACR only. A comparison between the test and CFD solution shows that the computation accurately predicted the ACR. The pressure recovery (PR), which is more sensitive to the flow condition, is off by about 5%.

VI. Conclusions

A full Navier-Stokes computation has been made for an axisymmetric scramjet inlet at Mach 5 using the USA-RG2 code. The multizone bookkeeping capability of the code allowed modeling of complex geometries, and computing mixed internal and external flows simultaneously. The flexibility of using different numerical schemes in different zones made it efficient to compute a flowfield with significantly different geometric scales and flow physics, such as the blunt centerbody nose and cowl leading edge.

The numerical solution in terms of wall static pressure and throat total pressure showed good agreement with the test data, especially upstream of the throat. Some disagreement downstream of the throat and in the throat core flow may be due to the relatively coarse grid used in the region. Other reasons that may contribute to the disagreement are the location of the boundary-layer transition and the turbulence model used.

The inlet performance was calculated by postprocessing the FNS solution. The air capture ratio was predicted to within 0.4% of the test data and the pressure recovery underpredicted by about 5%. In addition to ACR and PR, the postprocessor was able to provide other performance parameters useful for inlet design, such as kinetic energy efficiency, distortion parameters in the throat, etc.

Acknowledgments

This work was supported by NASP JPO under Contract F33657-91-C-2012. The author appreciates the technical support and consultation from his colleagues in the Rockwell Science Center CFD Department and Rocketdyne CFD Unit. The author would also like to thank Allen Goldman, Munir Sindir, and Gary Ratekin of Rocketdyne for their encouragement and support on this work.

References

[1]Dwoyer, D. L., and Kumar, A., "Computational Analysis of Hypersonic Airbreathing Aircraft Flow Fields," AIAA Paper 87-0279, Jan. 1987.

[2]Chakravarthy, S. R., Szema, K.-Y., and Haney, J. W., "Unified 'Nose-to-Tail' Computational Method for Hypersonic Vehicle Applications," AIAA Paper 88-2564, June 1988.

[3]Pearson, L. W., "Hypersonic Research Engine Project—Phase II A, Inlet Program Terminal Summary Report," The Garrett Corp., AiResearch Manufacturing Div., Rept. AP-69-4883, March 27, 1969; see also NASA CR 66797, 1969.

[4]Goldberg, U. C., Gorski, J. J., and Chakravarthy, S. R., "Afterbody Flowfield Computations at Transonic and Supersonic Mach Numbers," *Journal of Propulsion and Power*, Vol. 3, No. 1, 1987, p. 56–62.

[5]Chen, C. L., Ramakrishnan, S., Szema, K. Y., Dresser, H. S., and Rajagopal, K., "Multi-Zonal Navier-Stokes Solutions for the Multi-Body Space Shuttle Configuration," AIAA Paper 90-0434, Jan. 1990.

[6]Chakravarthy, S. R., Szema, K. Y., Goldberg, U. C., Gorski, J. J., and Osher, S., "Application of a New Class of High Accuracy TVD Schemes to the Navier-Stokes Equations," AIAA Paper 85-0165, Jan. 1985.

[7]Ota, D. K., and Chakravarthy, S. R., "An Equilibrium Air Navier-Stokes Code for Hypersonic Flows," AIAA Paper 88-0419, Jan. 1988.

[8]Palaniswamy, S., Chakravarthy, S. R., and Ota, D. K., "Finite Rate Chemistry for USA-Series Codes: Formulation and Applications," AIAA Paper 89-0200, Jan. 1989.

[9]Goldberg, U. C., "Turbulent Flow Computations with a Two-Time Scale One-Equation Model," AIAA Paper 91-1790, June 1991.

[10]Goldberg, U. C., "Separated Flow Treatment with a New Turbulence Model," *AIAA Journal*, Vol. 24, No. 10, 1986, pp. 1711–1713.

[11]Szema, K. Y., Chakravarthy, S. R., Riba, W. T., Byerly, J., and Dresser, H. S., "Multi-Zone Euler Marching Technique for Flow over Single and Multi-Body Configurations," AIAA Paper 87-0592, Jan. 1987.

[12]NASA Ames Research Staff, "Equations, Tables, and Charts for Compressible Flow," NACA Rept. 1135, 1935.

[13]Hsia, Y., Gross, B., and Ortwerth, J. P., "Inviscid Analysis of a Dual Mode Scramjet Inlet," *Journal of Propulsion and Power*, Vol. 7, No. 6, 1991, pp. 1030–1035.

[14]Hsia, Y., Daso, E. O., and Padhye, V. A., "Full Navier-Stokes Analysis of a Three-Dimensional Scramjet Inlet," *Journal of Propulsion and Power*, Vol. 8, No. 5, 1992, pp. 1071–1078.